Ultralow-Vertical-Current Magnetization Switching Effect in an All Van Der Waals 2D Heterostructure

Hao Wu(武浩)[1,2†], Li Yang(杨丽)[1,2†], Gaojie Zhang(张高节)[1,2], Wen Jin(靳雯)[1,2], Jie Yu(虞杰)[1,2], Bichen Xiao(肖碧晨)[1,2], Ahmed Annas(王绍凌)[1,2], Wenfeng Zhang(张文峰)[1,2,3], and Haixin Chang(常海欣)[1,2,3*]

[1]*Center for Joining and Electronic Packaging, State Key Laboratory of Material Processing and Die & Mold Technology, School of Materials Science and Engineering, Huazhong University of Science and Technology, Wuhan 430074, China*

[2]*Wuhan National High Magnetic Field Center and Institute for Quantum Science and Engineering, Huazhong University of Science and Technology, Wuhan 430074, China*

[3]*Shenzhen R&D Center of Huazhong University of Science and Technology, Shenzhen 518000, China*

(Received 25 September 2024; accepted manuscript online 7 January 2025)

The manipulation of magnetization and spin polarization using electrical currents represents a fundamental breakthrough in spintronics. It has formed the foundation for data storage and next-generation computing systems. Spin-transfer torque (STT) and spin-orbit torque (SOT) have emerged as prominent mechanisms in current-driven magnetization switching. However, these approaches typically require critical current densities in the range of 10^6 to 10^9 A·cm^{-2}, resulting in significant heat generation during data writing processes. Herein, we report the discovery of an ultralow-vertical-current magnetization switching effect in a van der Waals ferromagnetic/ferroelectric heterostructure based on the modulation of the critical magnetic field (H_C) using small vertical currents, with a critical current density as low as 1.81 A·cm^{-2} and an average effective field (H_{eff}/J_C) as high as 150.3 mT·A^{-1}·cm^2. This unique magnetization switching effect with ultralow-critical-vertical-current densities typically six to nine orders of magnitude lower than those of the STT and SOT provides a new transformative and viable pathway for developing next-generation spintronic and quantum technologies.

DOI: 10.1088/0256-307X/42/2/027502 CSTR: 32039.14.0256-307X.42.2.027502

1. Introduction. Magnetization switching through electrical currents has revolutionized the fields of spintronics and data storage, enabling the development of low-power, high-speed, and non-volatile chip technologies.[1–4] In current research, current-induced magnetization switching primarily relies on two mechanisms: spin-transfer torque (STT) and spin-orbit torque (SOT),[5,6] which represent cutting-edge methods for controlling magnetization states in nanostructures. These techniques demonstrate significant potential, particularly in the development of non-volatile memory systems, such as magnetic random-access memory (MRAM). However, they still encounter numerous technical challenges for widespread application. One of the most prominent challenges is the high critical current density (J_C) required for effective magnetization switching, typically ranging from 10^6 to 10^9 A·cm^{-2}.[7–9] Such a high J_C generates a large amount of heat during the switching process, which not only severely affects the energy efficiency of devices but also accelerates material degradation.[10] Significant efforts have been implemented to reduce the J_C required for magnetization switching. For example, reducing the perpendicular magnetic anisotropy (PMA) and coercivity of magnetic thin films can lower J_C to approximately 2×10^5 A·cm^{-2}.[11] Through the topologically protected large spin polarization of the type-II Weyl semimetal WTe_2, a J_C as low as $\sim 2.96\times10^5$ A·cm^{-2} has been achieved for magnetization switching in a Py/WTe_2 heterojunction.[12] Additionally, magnetization switching via SOT has been achieved in monolayer ferromagnetic semiconductor GaMnAs by eliminating bilayer structures, reducing J_C to $\sim 3.4\times10^5$ A·cm^{-2}.[13]

Recently, the discovery of high-temperature van der Waals ferromagnetic and ferroelectric materials has facilitated the development of artificial multiferroics, in which the electrical control of magnetization with significantly reduced energy consumption is more readily achievable.[14,15] The stacking of two-dimensional van der Waals ferromagnets with two-dimensional van der Waals ferroelectrics to form heterostructures is a viable approach to achieving magnetoelectric coupling.[16,17] In this letter, we describe the construction of a FGaT/CIPS heterostructure using the van der Waals materials Fe_3GaTe_2 (FGaT) and $CuInP_2S_6$ (CIPS). FGaT is a room-temperature van der Waals ferromagnetic material with a magnetic Curie temperature of 367 K,[18,19] whereas CIPS is a van der Waals layered ferroelectric material with a ferroelectric

†These authors contributed equally to this work.
*Corresponding author. Email: hxchang@hust.edu.cn
© 2025 Chinese Physical Society and IOP Publishing Ltd. All rights, including for text and data mining, AI training, and similar technologies, are reserved.

transition temperature of 320 K.[20] The magnetoelectric transport properties of the FGaT/CIPS heterostructure under an ultralow vertical current were investigated, including H_C, magnetic anisotropy, and the magnetization switching effect induced by the ultralow vertical current.

2. Results and Discussions. Figure 1(a) shows a schematic of the FGaT/CIPS heterostructure device, which comprises two configurations. One is a Hall device designed to measure the longitudinal and anomalous Hall resistances; the other is a vertical current/bias electrode used to apply a vertical current or bias to the FGaT/CIPS heterostructure, with graphene serving as the conductive top electrode. Figure 1(b) depicts an actual microscopic optical image of the FGaT/CIPS heterostructure device, where the thicker h-BN serves as an electrical insulator, preventing direct contact between the graphene and underlying Au electrodes. Figure 1(c) presents an atomic force microscopy (AFM) image of the overlapping region between the graphene electrode and CIPS in the FGaT/CIPS heterostructure device, and the height profile along the white dashed line is shown in Fig. 1(d). In this region, the CIPS layer has a thickness of 21.43 nm, corresponding to approximately 31 layers, whereas the graphene layer has a thickness of 5.21 nm, corresponding to approximately 15 layers. An AFM image captured at the center of the FGaT/CIPS heterostructure device is shown in Fig. 1(e), where the FGaT nanosheet has a thickness of approximately 19.75 nm, which is equivalent to approximately 24 layers [Fig. 1(f)].

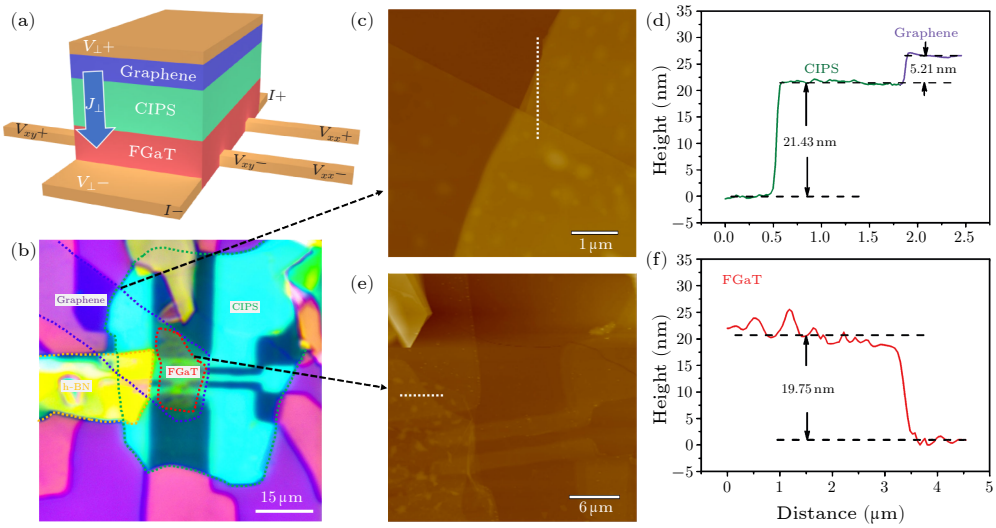

Fig. 1. (a) Schematic of the FGaT/CIPS Hall device with vertical-current electrodes. (b) Optical microscope image of the FGaT/CIPS heterostructure device. (c) AFM image of the overlap of graphene and CIPS as indicated by the black arrow in (b). (d) AFM height profile along the white dashed line in (c). (e) AFM image of FGaT at the center of the FGaT/CIPS Hall device as indicated by the black arrow in (b). (f) AFM height profile along the white dashed line in (e).

Prior to exfoliation, the FGaT crystal used in the FGaT/CIPS device was magnetically characterized, as shown in Figs. 2(a) and 2(b). Figure 2(a) shows the thermomagnetic curves of the FGaT crystal under a vertical magnetic field of 0.1 T [zero-field cooling (ZFC) and field cooling (FC)], whereas Fig. 2(b) shows the magnetic hysteresis loops measured at various temperatures. These figures show that the Curie temperature of the FGaT crystal is approximately 358 K. The saturation magnetization at room temperature (300 K) is 46.75 emu/g, whereas, at a low temperature (2 K), it reaches 66.70 emu/g, which is consistent with previous reports.[18,21] The FGaT/CIPS heterostructure retains metallic properties similar to those of the pristine FGaT nanosheet, as shown in Fig. 2(c).[18] Figure 2(d) depicts the temperature dependence of the anomalous Hall resistance under a vertical magnetic field of 0.1 T, indicating that the Curie temperature of the FGaT/CIPS heterostructure is also 358 K, which is consistent with that of the bulk material. Figures 2(e) and 2(f) show the hysteresis loops of the anomalous Hall resistance as a function of the magnetic field at different temperatures ranging from 2 to 400 K. As the temperature increases, the H_C of the FGaT/CIPS heterostructure gradually decreases, retaining a H_C of 18.7 mT at 350 K. At 400 K, the anomalous Hall effect, characterized by the shape of the hysteresis loops, disappears, and only the linear normal Hall effect remains. At temperatures of 300 K and below, the hysteresis loops of the anomalous Hall resistance as a function of the magnetic field exhibit a highly rectangular shape, indicating that the FGaT/CIPS heterostructure has strong perpendicular magnetic anisotropy, which is also evident in Fig. 3. Figures 3(a)–3(d) show the anomalous Hall resistance of the FGaT/CIPS heterostructure under an in-plane magnetic field at various temperatures. The magnetic field indicated by arrows represents the magnetic anisotropy field (H_K), which is the field required to fully switch the magnetization to the hard axis (in-plane direction). At H_K, the Hall resistance should be nearly zero and remain unchanged as the external magnetic field increases. The mag-

netic anisotropy fields of the FGaT/CIPS heterostructure at 2, 100, 200, and 300 K were determined to be 9.29, 7.76, 6.12, and 3.40 T, respectively. Based on these values, the perpendicular magnetic anisotropy energy density (K_u) of FGaT within the FGaT/CIPS heterostructure was calculated using the relation $K_u = M_S H_K/2$, where M_S is the saturation magnetization of FGaT (Table S1). The calculated values of K_u at 2, 100, 200, and 300 K were 2.27, 1.81, 1.30, and 0.58 MJ/m^3, respectively, all of which exceed the previously reported values.[18,22]

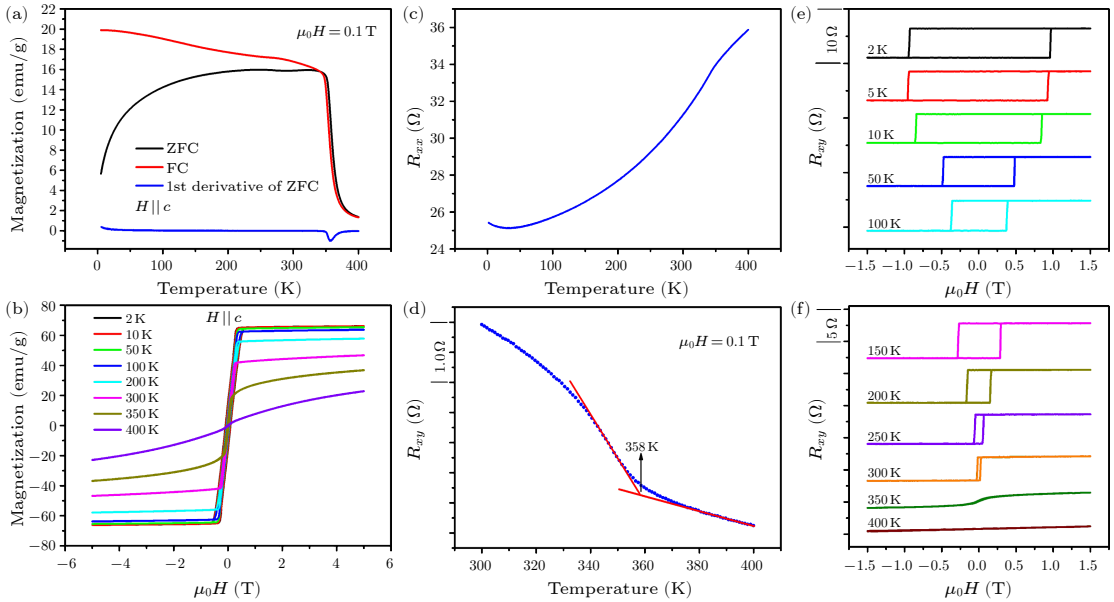

Fig. 2. Magnetic and electrical transport properties. (a) ZFC and FC curves of FGaT crystals in the temperature range of 5–400 K when a magnetic field of 0.1 T is applied. (b) Hysteresis loops of FGaT crystals at different temperatures from 2 to 400 K. (c) Temperature-dependent longitudinal resistance (R_{xx}) of the FGaT/CIPS heterostructure from 2 to 400 K. (d) Temperature-dependent Hall resistance (R_{xy}) of the FGaT/CIPS heterostructure from 300 to 400 K. (e), (f) R_{xy} as a function of magnetic field of the FGaT/CIPS heterostructure at different temperatures from 2 to 400 K. All tests were conducted with the c-axis parallel to the magnetic field direction.

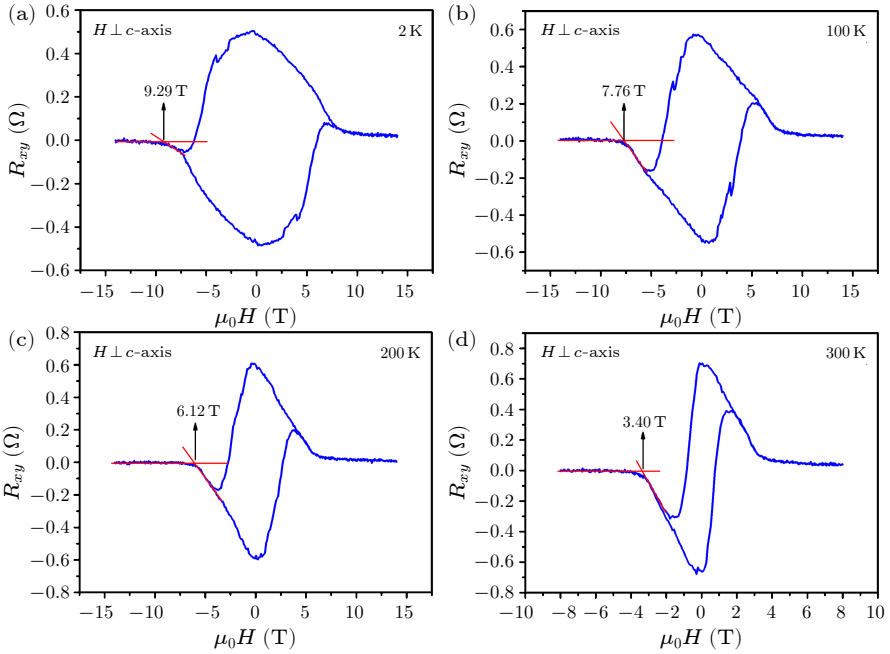

Fig. 3. Magnetic anisotropy of the FGaT/CIPS heterostructure. (a)–(d) Magnetic field-dependent Hall resistance in the in-plane configuration at temperatures of 2 K (a), 100 K (b), 200 K (c), and 300 K (d).

Importantly, we observed that an ultralow vertical current modulates the H_C of the FGaT/CIPS heterostructure. Figure 4(a) shows the anomalous Hall resistance hysteresis loops of the FGaT/CIPS heterostructure at 2 K under different vertical currents. H_C reaches its maximum when the vertical current is zero. However, when

a small positive or negative vertical current is applied, H_C decreases rapidly. To eliminate potential randomness, we measured the Hall resistance hysteresis loops at each vertical current density five times, as shown in Fig. 4(b). The corresponding statistical results for H_C are shown in Fig. 4(c). H_C reaches its maximum at zero vertical current, with an average value of approximately 872 mT. When $J_\perp = -12.35\,\mathrm{A{\cdot}cm^{-2}}$, H_C decreases rapidly to 511.6 mT, a reduction of 360.4 mT. As the current is further increased, the decreasing trend of H_C gradually slows. For instance, when $J_\perp$ increases to $-30.98\,\mathrm{A{\cdot}cm^{-2}}$, H_C decreases by only 82.5 mT. The Hall resistance hysteresis loops under an in-plane magnetic field with different vertical-current densities are shown in Fig. 4(d). The hysteresis loops under various vertical currents are nearly identical, indicating that the H_K remains unchanged. This suggests that the magnetic anisotropy is not affected by the applied small vertical current. This ultralow-vertical-current-controlled H_C can be used to modulate magnetization switching. As shown in Fig. 4(e), at a vertical magnetic field of ± 0.6 T (272 mT away from H_C), the critical current density for magnetization switching is as low as $1.81\,\mathrm{A{\cdot}cm^{-2}}$. The current density required for complete magnetization switching is only $3.09\,\mathrm{A{\cdot}cm^{-2}}$, meaning that a critical vertical current (J_C) of $1.81\,\mathrm{A{\cdot}cm^{-2}}$ is equivalent to a vertical magnetic field (H_{eff}) of 272 mT. The average effective field (H_{eff}/J_C) is approximately $150.3\,\mathrm{mT{\cdot}A^{-1}{\cdot}cm^2}$. The current density required for vertical-current-driven magnetization switching in the FGaT/CIPS heterostructure is significantly lower than that in conventional STT or SOT mechanisms, which typically demand current densities in the range of 10^6 to 10^9 $\mathrm{A{\cdot}cm^{-2}}$.[7–9] Notably, previous studies have reported similar in-plane current-induced modulations of H_C and current-controlled magnetization switching in pristine FGaT nanosheets, which require a J_C of $7.31 \times 10^5\,\mathrm{A{\cdot}cm^{-2}}$,[22] which is still over five orders of magnitude higher than the J_C observed in FGaT/CIPS heterostructures. Furthermore, for state-of-the-art SOT devices with high switching efficiencies, the typical average effective field ranges from approximately 10^{-9} to $10^{-6}\,\mathrm{mT{\cdot}A^{-1}{\cdot}cm^2}$.[23–25] In contrast, the efficiency of ultralow-vertical-current magnetization switching in the FGaT/CIPS heterostructure is 8 to 11 orders of magnitude higher. Note that, owing to the ferroelectric properties of CIPS, voltage effects may contribute to the magnetization switching in the FGaT/CIPS heterostructure. To clarify this, we compared the unnormalized current- and voltage-driven anomalous Hall resistance switching data [Figs. S1(a) and S1(b)]. As shown in Fig. S1(a), the small vertical currents required for magnetization switching under the positive and negative magnetic fields are symmetric in magnitude, whereas the corresponding vertical voltages are random and asymmetric [Fig. S1(b)]. Hence, at 2 K, the dominant mechanism for magnetization switching in the FGaT/CIPS heterostructure is attributed to the small vertical current. The cyclic $J_\perp$–$V_\perp$ curve [Fig. 4(f)] shows the vertical voltage required to apply different vertical currents to the FGaT/CIPS heterostructure at 2 K, where only p–n junction-like characteristics are observed without any hysteresis loops within our voltage testing range.

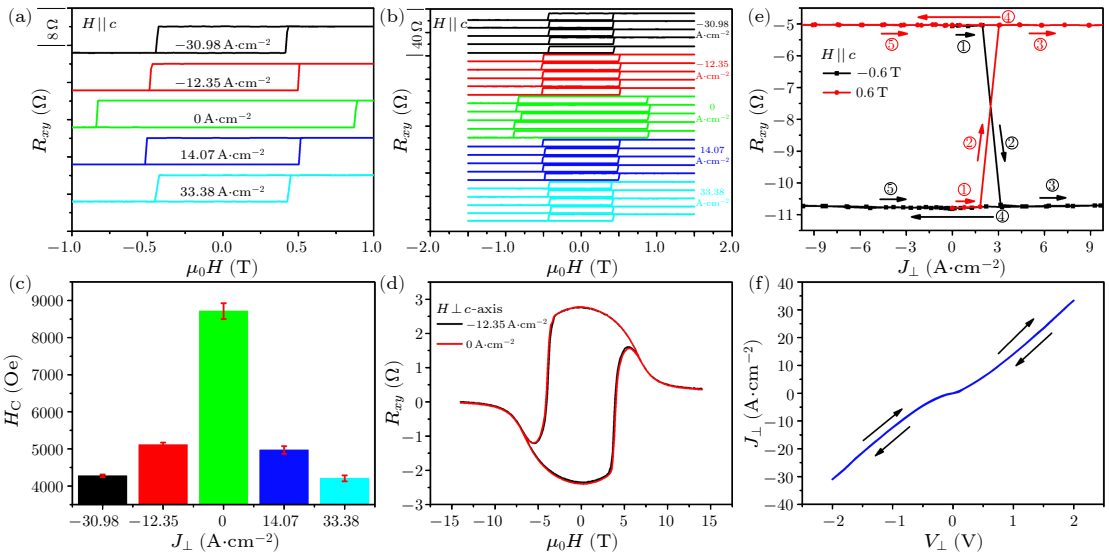

Fig. 4. Ultralow-vertical-current magnetization switching effect in the FGaT/CIPS heterostructure at 2 K. Anomalous Hall effect (a) and reproducibility test (b) under different applied vertical currents. (c) Statistical variation in H_C with vertical-current density. (d) Variation in anomalous Hall resistance with in-plane magnetic field under different applied vertical currents. (e) Regulation of anomalous Hall resistance by applied vertical current under ± 0.6 T out-of-plane magnetic fields, where the circled numbers indicate the order of the current sweep. (f) Cyclic $J_\perp$–$V_\perp$ curve at zero magnetic field.

The magnetization switching effect of the FGaT/CIPS heterostructure with a small vertical current at 200 K is shown in Fig. 5. Unlike the behavior observed at 2 K, the switching effect on the vertical current at 200 K exhibits directionality: H_C decreases with a negative current and increases with a positive current [Fig. 5(a)]. Similar to 2 K, the Hall resistance hysteresis loops in the in-plane magnetic field with different vertical currents exhibit no no-

ticeable differences [Fig. 5(b)], indicating that the H_K and magnetic anisotropy remain unchanged. As the decrease in H_C occurs only in the negative vertical-current direction, the Hall resistance does not switch during the initial scan from zero to a positive current. Hall resistance switching occurs only when scanning in the negative current direction. Under vertical magnetic fields of ±145 mT, the critical current density required for magnetization switching is $-24.3\,\mathrm{A{\cdot}cm^{-2}}$, whereas that required for complete switching is $-26.3\,\mathrm{A{\cdot}cm^{-2}}$ [Fig. 5(c)]. At 200 K, the H_C of the FGaT/CIPS heterostructure is 161.5 mT, meaning that a vertical current of $-24.3\,\mathrm{A{\cdot}cm^{-2}}$ is equivalent to a vertical magnetic field of 16.5 mT. Compared with the behavior at 2 K, the effect of a small vertical current on modulating H_C and switching magnetization in the FGaT/CIPS heterostructure is significantly reduced. Furthermore, we present unnormalized current- and voltage-driven anomalous Hall-resistance switching data at 200 K [Figs. S1(c) and S1(d)]. The vertical current [Fig. S1(c)] and vertical voltage [Fig. S1(d)] required for magnetization switching under positive and negative magnetic fields are both equal in magnitude and symmetric. Therefore, the role of the vertical voltage in inducing magnetization switching in the FGaT/CIPS heterostructure at 200 K remains to be further verified and discussed. The cyclic $J_\perp$–$V_\perp$ curve [Fig. 5(d)] shows the vertical voltage required to apply various vertical currents to the FGaT/CIPS heterostructure at 200 K. Similar to the results at 2 K, the FGaT/CIPS exhibits only weak p–n junction-like characteristics with no hysteresis loops observed in the tested voltage range at 200 K. Additionally, we attempted to measure the ultralow-vertical-current magnetization switching effect in the FGaT/CIPS heterostructure at higher temperatures. However, no magnetization switching effect was observed at room temperature.

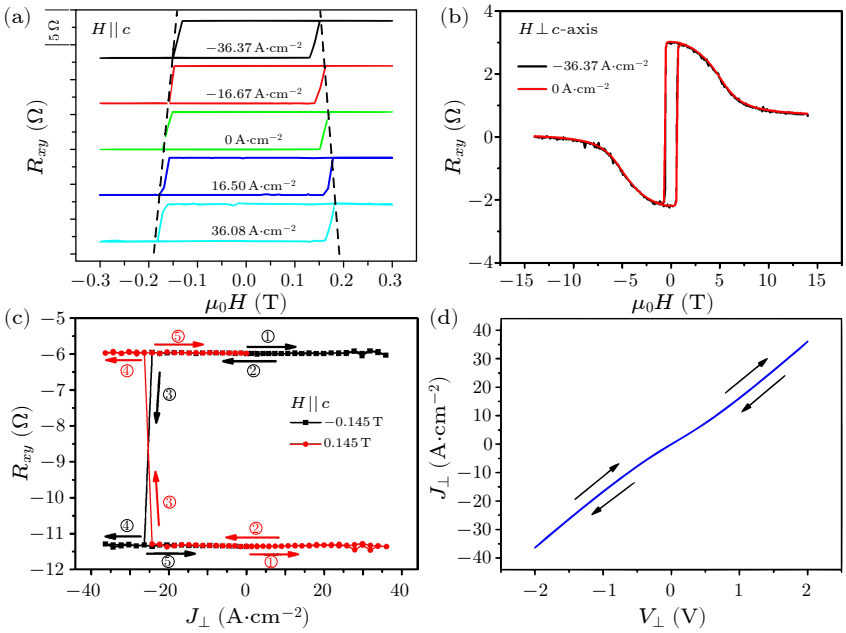

Fig. 5. Ultralow-vertical-current magnetization switching effect in the FGaT/CIPS heterostructure at 200 K. (a) Variation in the anomalous Hall resistance with out-of-plane magnetic field under different applied vertical currents. (b) Variation in the anomalous Hall resistance with in-plane magnetic field under different applied vertical currents. (c) Regulation of anomalous Hall resistance by applied vertical current under ±0.145 T out-of-plane magnetic fields, where the circled numbers indicate the order of the current sweep. (d) Cyclic $J_\perp$–$V_\perp$ curve at zero magnetic field.

The ultralow-vertical-current-driven magnetization switching effect observed in the FGaT/CIPS heterostructure fundamentally relies on the modulation of H_C by the applied current. As a complex non-intrinsic magnetic parameter, the variation in H_C may be influenced by several contributing factors. For instance, current or electric fields can alter the magnetic anisotropy, thereby affecting the magnitude of H_C.[26] However, our experimental results indicate that the magnetic anisotropy remains unchanged. Additionally, thermal effects and ferromagnetic fluctuations can influence the magnitude of H_C. Nevertheless, in addition to the observed switching, no thermal drift in the Hall resistance is detected as the current increases [Figs. 4(e) and 5(c)], thus excluding the influence of Joule heating effect. The variation in H_C owing to ferromagnetic fluctuations is typically more pronounced near the Curie temperature. However, in contrast to this expectation, our experimental results show that the current modulation effect is significantly stronger at the extremely low temperature of 2 K than at 200 K, thus excluding the influence of magnetic fluctuation effects. The overlap of the electron wavefunctions in the vertical direction can alter the interlayer exchange coupling and free energy,[27,28] which can affect the magnitude of H_C. Specifically, the current can excite spin waves that influence H_C. Theories and experiments have established that spin waves can be excited by a current.[29,30] This is crucial for the magnetization switching process because spin waves facilitate the

movement of magnetic domain walls, thus promoting magnetization switching.[31,32] Notably, the graphene electrode may also provide a spin-polarized current,[33,34] which is frequently used as a source of spin-wave excitation.[35,36] The heterojunction formed by CIPS and FGaT can also break the symmetry of FGaT, thereby generating DMI and topological magnetic defects, which can serve as sources of spin-wave excitation.[37]

3. Conclusion. We observed an ultralow-vertical-current magnetization switching effect in an FGaT/CIPS van der Waals heterostructure. The J_C required to switch the magnetization of the FGaT/CIPS heterostructure is as low as $1.81\,\mathrm{A{\cdot}cm^{-2}}$ at 2 K, which is six to nine orders of magnitude lower than that required for conventional current-driven STT or SOT magnetization switching, representing a record-low critical current density to date. As the temperature increases, this current modulation effect weakens slightly at 200 K. This unique magnetization switching effect can inspire the development of next-generation low-power, high-efficiency spintronic devices and create the foundation for innovations in magnetic data storage and logic devices.

Acknowledgements. This work was supported by the National Key Research and Development Program of China (Grant No. 2022YFE0134600), the Interdisciplinary Research Program of Huazhong University of Science and Technology (Grant No. 2023JCYJ007), the China Postdoctoral Science Foundation (Grant No. 2022M711234), the National Natural Science Foundation of China (Grant Nos. 52272152, 61674063, and 62074061), the Natural Science Foundation of Hubei Province, China (Grant No. 2022CFA031), and the Foundation of Shenzhen Science and Technology Innovation Committee (Grant Nos. JCYJ20180504170444967, JCYJ20210324142010030, and JCYJ20230807143614031).

References

[1] Higo T, Kondou K, Nomoto T, Shiga M, Sakamoto S, Chen X, Nishio-Hamane D, Arita R, Otani Y, Miwa S, and Nakatsuji S 2022 *Nature* **607** 474
[2] Xue F, Lin S J, Song M, Hwang W, Klewe C, Lee C M, Turgut E, Shafer P, Vailionis A, Huang Y L, Tsai W, Bao X, and Wang S X 2023 *Nat. Commun.* **14** 3932
[3] Liu L, Qin Q, Lin W, Li C, Xie Q, He S, Shu X, Zhou C, Lim Z, Yu J, Lu W, Li M, Yan X, Pennycook S J, and Chen J 2019 *Nat. Nanotechnol.* **14** 939
[4] Li W, Zhu W, Zhang G, Wu H, Zhu S, Li R, Zhang E, Zhang X, Deng Y, Zhang J, Zhao L, Chang H, and Wang K 2023 *Adv. Mater.* **35** 2303688
[5] Grimaldi E, Krizakova V, Sala G, Yasin F, Couet S, Sankar Kar G, Garello K, and Gambardella P 2020 *Nat. Nanotechnol.* **15** 111
[6] Kumar P and Naeemi A 2022 *Appl. Phys. Lett.* **121** 112406
[7] Miron I M, Garello K, Gaudin G, Zermatten P J, Costache M V, Auffret S, Bandiera S, Rodmacq B, Schuhl A, and Gambardella P 2011 *Nature* **476** 189
[8] Wang X, Wu H, Qiu R, Huang X, Zhang J, Long J, Yao Y, Zhao Y, Zhu Z, Wang J, Shi S, Chang H, and Zhao W 2023 *Cell Rep. Phys. Sci.* **4** 101468
[9] Myers E B, Ralph D C, Katine J A, Louie R N, and Buhrman R A 1999 *Science* **285** 867
[10] Fong X, Kim Y, Venkatesan R, Choday S H, Raghunathan A, and Roy K 2016 *Proc. IEEE* **104** 1449
[11] Shi G, Chang Y, Cai J, Zhang P, Pan F, and Song C 2017 *Jpn. J. Appl. Phys.* **56** 100303
[12] Shi S, Liang S, Zhu Z, Cai K, Pollard S D, Wang Y, Wang J, Wang Q, He P, Yu J, Eda G, Liang G, and Yang H 2019 *Nat. Nanotechnol.* **14** 945
[13] Jiang M, Asahara H, Sato S, Kanaki T, Yamasaki H, Ohya S, and Tanaka M 2019 *Nat. Commun.* **10** 2590
[14] Long J, Ivanov M S, Khomchenko V A, Mamontova E, Thibaud J M, Rouquette J, Beaudhuin M, Granier D, Ferreira R A S, Carlos L D, Donnadieu B, Henriques M S C, Paixão J A, Guari Y, and Larionova J 2020 *Science* **367** 671
[15] Xu S, Wang J, Chen P, Jin K, Ma C, Wu S, Guo E, Ge C, Wang C, Xu X, Yao H, Wang J, Xie D, Wang X, Chang K, Bai X, and Yang G 2023 *Nat. Commun.* **14** 2274
[16] Gong C and Zhang X 2019 *Science* **363** eaav4450
[17] Valencia S, Crassous A, Bocher L, Garcia V, Moya X, Cherifi R O, Deranlot C, Bouzehouane K, Fusil S, Zobelli A, Gloter A, Mathur N D, Gaupp A, Abrudan R, Radu F, Barthélémy A, and Bibes M 2011 *Nat. Mater.* **10** 753
[18] Zhang G, Guo F, Wu H, Wen X, Yang L, Jin W, Zhang W, and Chang H 2022 *Nat. Commun.* **13** 5067
[19] Zhang G, Luo Q, Wen X, Wu H, Yang L, Jin W, Li L, Zhang J, Zhang W, Shu H, and Chang H 2023 *Chin. Phys. Lett.* **40** 117501
[20] Liu F, You L, Seyler K L, Li X, Yu P, Lin J, Wang X, Zhou J, Wang H, He H, Pantelides S T, Zhou W, Sharma P, Xu X, Ajayan P M, Wang J, and Liu Z 2016 *Nat. Commun.* **7** 12357
[21] Zhang G, Yu J, Wu H, Yang L, Jin W, Zhang W, and Chang H 2023 *Appl. Phys. Lett.* **123** 101901
[22] Zhang G, Wu H, Yang L, Jin W, Xiao B, Zhang W, and Chang H 2024 *ACS Mater. Lett.* **6** 482
[23] Yang Y, Xu Y, Zhang X, Wang Y, Zhang S, Li R W, Mirshekarloo M S, Yao K, and Wu Y 2016 *Phys. Rev. B* **93** 094402
[24] Wu H, Zhang P, Deng P, Lan Q, Pan Q, Razavi S A, Che X, Huang L, Dai B, Wong K, Han X, and Wang K L 2019 *Phys. Rev. Lett.* **123** 207205
[25] Zhao T, Liu L, Zhou C, Zheng Z, Li H, Xie Q, Yao B, Ren L, Chai J, Dong Z, Zhao C, and Chen J 2023 *Adv. Mater.* **35** 2208954
[26] Sivadas N, Okamoto S, and Xiao D 2016 *Phys. Rev. Lett.* **117** 267203
[27] Jiang S, Shan J, and Mak K F 2018 *Nat. Mater.* **17** 406
[28] Gao S, Yang L, and Spataru C D 2017 *Nano Lett.* **17** 7809
[29] Hillebrands B 1990 *Phys. Rev. B* **41** 530
[30] Xi H, Yang Y, Ouyang J, Shi Y, and Gao K Z 2007 *Phys. Rev. B* **75** 174411
[31] Wang X S, Yan P, Shen Y H, Bauer G E W, and Wang X R 2012 *Phys. Rev. Lett.* **109** 167209
[32] Kammerer M, Stoll H, Noske M, Sproll M, Weigand M, Illg C, Woltersdorf G, Fähnle M, Back C, and Schütz G 2012 *Phys. Rev. B* **86** 134426
[33] Lin X, Su L, Si Z, Zhang Y, Bournel A, Zhang Y, Klein J O, Fert A, and Zhao W 2017 *Phys. Rev. Appl.* **8** 034006
[34] Panda J, Ramu M, Karis O, Sarkar T, and Kamalakar M V 2020 *ACS Nano* **14** 12771
[35] Slonczewski J C 1999 *J. Magn. Magn. Mater.* **195** L261
[36] Pribiag V S, Krivorotov I N, Fuchs G D, Braganca P M, Ozatay O, Sankey J C, Ralph D C, and Buhrman R A 2007 *Nat. Phys.* **3** 498
[37] Wang Y, Wang J, Kitamura T, Hirakata H, and Shimada T 2023 *Acta Mater.* **250** 118867